Journal of Operation and Automation in Power Engineering

Vol. 14, No. 4, Dec. 2026, Pages: 249-256

http://joape.uma.ac.ir

Research Paper

Design and Analysis of BLDC Motor with Novel Hybrid Approach for Cogging Torque Reduction

Tanuj Jhankal and *Amit N. Patel* *

Department of Electrical, Institute of Technology, Nirma University, Ahmedabad, Gujarat, India.

Abstract— *Radial flux brushless DC motors with surface-mounted permanent magnets offer several advantages, but they are also characterized by a significant drawback: high cogging torque. Mitigating cogging torque is a critical challenge in the design of brushless direct current motors, particularly in applications such as electric vehicles. This article presents three approaches to reduce cogging torque in radial flux permanent magnet brushless motors: teeth edge inset width variation, magnet tip depth variation, and a hybrid approach combining both techniques. The teeth edge inset width variation method involves reducing the inset width of the stator teeth, while the magnet tip depth variation approach addresses the depth of the magnet's edge inset on the rotor core surface. The hybrid approach integrates changes to both the stator teeth and rotor magnet poles. Additionally, the study investigates how these approaches affect the average torque and flux density distribution. Finite element analysis was conducted to simulate and analyze a 1000 W, 510 rpm radial flux brushless DC motor. The results show that the proposed methods effectively reduce cogging torque, demonstrating their potential to enhance the performance of these motors in practical applications.*

Keywords—Cogging torque, electromagnetic analysis, finite element analysis, brushless DC motor, low speed electrical vehicle application.

NOMENCLATURE

α_{ph}	Number of phases
ϕ	Flux in the magnetic circuit
ϕ_{gap}	Air-gap flux
θ_r	Rotor angle
θ_{sk}	Optimal skew angle
A_{cond}	Cross-sectional area of each
A_{slot}	Area of slot of the proposed motor
ac	Slot-specific loading
$B_{air-gap}$	Specific magnetic loading
D	Bore diameter
d_s	Depth of slot
D_{ro}	Outer rotor diameter
Dso	Outer diameter
I	Current
K_w	Winding factor
MTD	Magnet tip depth
N_c	Number of coils conducting simultaneously
N_s	Number of slots
N_{pm}	Number permanent magnet poles on the rotor
n_{ps}	Pitch shortening
N_{tph}	Number of turns per phase
$NdFeB$	Neodymium iron boron
PM	Permanent magnet
R_{gap}	Air-gap reluctance
R_{ro}	Outer radius of the rotor
R_{si}	Stator inner radius
R_{so}	Stator outer radius
RF	Radial flux
$RF-BLDC$	Radial flux brushless direct current
SPM	Surface permanent magnet
$TEIW$	Tooth edge inset width
w_t	Width of the stator teeth
w_{bi}	Width of stator back iron
η_o	Desired motor efficiency

Received: 09 Jul. 2024
Revised: 05 Dec. 2024
Accepted: 07 Dec. 2024
*Corresponding author:
E-mail: amit.patel@nirmauni.ac.in (A.N. Patel)
DOI: 10.22098/joape.2025.15392.2182

1. INTRODUCTION

Radial flux brushless DC (RF-BLDC) motors are gaining popularity in transportation, residential, and industrial applications due to their superior operational efficiency, compact size, fast dynamic response, wide speed range, compatibility with solar-powered systems, and flexibility in control [1, 2]. Permanent magnet brushless motors can be classified into two main types: radial flux (RF) and axial flux motors. The key distinction between these types lies in the direction of the magnetic flux flow: in radial flux motors, the flux is radial to the machine's rotating axis, whereas in axial flux motors, the flux is parallel to the axis. The cylindrical shape of radial flux motors is particularly advantageous for low-speed applications, such as electric vehicles, where they offer significant benefits in terms of efficiency and design [3, 4]. RF-BLDC motors can be further categorized based on the number of rotating and stationary parts and their arrangement. These categories include inner runner, outer runner, dual stator, and dual rotor designs.

It is crucial to achieve low cogging torque in RF-BLDC motors for torque-sensitive applications like electric vehicles, robotics,

submarines, etc. One of the primary reasons for generating overall torque ripple, which decorates the performance of the motor, is cogging torque. Therefore, it is crucial to minimise this parasitic torque while designing RF-BLDC motors [5, 6]. The interaction between the magnetic flux set up by the permanent magnet (PM) and the stator teeth is known as cogging torque [7]. As the flux always favours a path with the least amount of reluctance, PM flux has a tendency to pass through the stator teeth, which causes an undesirable torque to be generated. Cogging torque creates speed and torque ripple, resulting in vibration and acoustic noise specifically for low-speed applications [8]. Reduction of cogging torque improves the overall performance of the motor. Many authors have suggested techniques to tackle this issue of cogging torque reduction. A few techniques are suitable for RF-BLDC motors and axial flux BLDC motors. Cogging torque reduction can be performed by changing the stator or changing the permanent magnets on the rotor. Cogging torque is also influenced by the selection of slot count and pole count of permanent magnet motors. Skewing is one of the basic techniques to minimise cogging torque [9], but it has a limitation of high radial thrust generation. Magnet displacement is the technique for reducing the cogging torque of radial and axial flux motors [10]. A slot displacement technique has been proposed for 5.0 kW 8-pole radial flux motors in [11], but this approach reduced useful torque too and increased the complexity of manufacturing the motor. The asymmetrical pole shaping technique is proposed in [12], and the conventional skewing with Herringbone design arrangement is presented in [13]. In [14], surface-mounted radial magnets, magnetic field distribution across the air-gap is not uniform with minimum efficiency in operation; an imbalance of air-gap can lead to high torque ripple. In [15], surface-mounted multilayer radial magnets minimise the magnetic flux leakage between layers, which can reduce the motor efficiency. In [16], the axial segments pole approach is presented, where the segment width is optimised to obtain the optimal pole shape. The segmented magnet arrangement leads to a substantial decrease in cogging force and improves the back-EMF waveform, which is beneficial for improving the performance and efficiency of the machine. But it also has several disadvantages, such as complex design, the need for a fast and accurate 2D analytical method combined with a quasi-3D approach for optimisation, which increases the computational burden, potentially requiring more time and resources, and sensitivity to optimisation accuracy. A slot shaping approach is presented in [17]; the combined approach of using a genetic algorithm and finite element method effectively reduces torque ripple to 4%, leading to smoother motor operation. While the study provides valuable insights into RF-BLDC motor design, the findings may need further validation for different motor configurations or operating conditions to ensure their applicability across various scenarios. Although torque ripple was effectively reduced, the study primarily focused on this aspect, potentially overlooking other performance metrics that could benefit from optimisation.

This paper emphasises the minimisation of the cogging torque of RF-BLDC motor with three proposed approaches. When utilising different PM shapes to get the desired outcomes, it is always desirable to either reduce the PM requirement or keep it the same as the benchmark design. Diminish torque fluctuations while minimising cogging torque and achieving improved performance at a lower cost of permanent magnets are the aim of this research, as several studies are discussed in the above paragraph which reduce the cogging torque, reduce the requirement of permanent magnet material and performance improvement of motors but are unable to obtain the simultaneous optimisation of all the parameters. Hence, three different approaches are proposed in this article to overcome this. Variations in magnet tip depth (MTD) and tooth edge inset width (TEIW) in RF-BLDC motors can lead to a reduction of cogging torque. A hybridisation of two approaches is also presented, which provides better performance than two individual approaches and allows the researchers to obtain a reduction in cogging torque and permanent magnet weight reduction simultaneously without extensive alteration of any one of the design parameters. By changing the teeth' edge shape radially, the TEIW configuration is realised. Electromagnetic analysis is performed on every configured design. After the electromagnetic analysis, it was determined that the RF-BLDC motor design featuring a hybridisation of TEIW variation and MTD variation exhibits superior electromagnetic performance in terms of reducing cogging torque.

The flow of the paper is as follows: In section 2, the design of the reference radial flux surface permanent magnet type (SPM-type) BLDC motor is presented. A discussion of cogging torque in RF-BLDC motor is presented in Section 3. In Section 4, the effectiveness of the proposed approaches is validated by comparing the results with the reference model, while the performance comparison is presented in Section 5, and Section 6 presents the conclusion.

2. Design of Proposed RF-BLDC Motor

The construction of an RF-BLDC motor is a testament to the fusion of modern engineering and technological ingenuity. At its core, this motor resembles its traditional counterparts but has a key differentiator: the absence of brushes and commutators. The stator is made of laminated cores housing the stationary windings meticulously placed in a radial pattern, which creates the magnetic field essential for motor operation. The rotor is located inside the stationary part. It is equipped with robust permanent magnet poles made from Neodymium Iron Boron (NdFeB) arranged to create a strong magnetic field when the rotor rotates.

The design of the RF-BLDC motor demands thorough attention due to numerous design constraints. It encompasses four main steps for its design. The main dimensions are calculated, including the outer diameter of the motor (D_{so}), length (L), and outer rotor diameter (D_{ro}). Various design variables are assumed to calculate the main dimensions, i.e. winding factor, pole pitch, specific loading, slot packing factor, average flux density, split ratio, aspect ratio, etc. [18–20]. After calculating the main dimensions, the stator design is carried out. Designing of the stator includes the calculations of slot dimensions (i.e. slot width, slot area, slot depth, slot opening), stator back iron width, tooth width, tooth tang depth and tooth tang angle are the significant dimensions of the stator [21]. Now, for the design of the rotor, selecting the number of PM poles in the RF-BLDC motor is essential. It depends upon factors like rotation speed, rotor topology used, iron loss, availability, and cost [22]. The proper selection of PM poles is vital to achieving good torque quality. For this design, a 0.5 mm air-gap length is considered. After calculating the main dimensions, stator design and rotor design, the fourth step is performance estimation. This RF-BLDC design stage is crucial as it estimates the motor performance based on the above-calculated design information. This is done to check the motor performance in terms of efficiency, losses, temperature rise and flux density in various parts of the motor. If the performance of the motor does not match the desired performance, adequate modifications have to be made to the design.

The proposed design uses M19 electrical steel material to create the rotor and stator core, while NdFeB grade 35 is used for PM pole creation. The air gap in the proposed motor, which is kept at 0.5 mm, plays a crucial role in the motor's performance. All the dimensions discussed above are calculated from specific relations, and the torque developed by the motor can be calculated using Eq. (1).

$$T_d = \frac{\eta_0 \omega_r a c R_{ro} k_w N_s N_c L}{\alpha_{ph} B_{air-gap}} \tag{1}$$

Where, $B_{air-gap}$ is the specific magnetic loading, N_c is the number of coils conducting simultaneously, α_{ph} represents the

number of phases, N_s is the number of slots, k_w is the winding factor, η_o is the desired motor efficiency, R_{ro} outer radius of the rotor and ac is the slot-specific loading [23].

$$D_{so} = \sqrt{\frac{2T_d}{\pi a c k_w k_s L (Split\ Ratio)^2 B_{air-gap}}} \tag{2}$$

$$ac = \frac{2\alpha_{ph} N_{tph} I}{\pi D_{ro}} \tag{3}$$

$$B_{air-gap} = \frac{N_{pm}\phi}{\pi D_{ro} L} \tag{4}$$

Here, N_{pm} is the number permanent magnet poles on the rotor, I is the current, N_{tph} is the number of turns per phase, and φ is the flux in the magnetic circuit. The k_w can be expressed using the Eq. (5). Where y_c is the ratio of N_s to N_{pm}, N_{ps} is the pitch shortening, and θ_{sk} is the optimal skew angle.

$$k_w = \frac{2\alpha \sin\left(\frac{\pi}{2y_c}.(y_c - n_{ps})\right) \sin\left(\frac{\pi\theta}{2}\right) \sin\left(\frac{\pi}{2\alpha}\right)}{\pi y_c \theta_{sk} \sin\left(\frac{\pi}{2y_c}\right)} \tag{5}$$

Using the Eqs. (3), (4) and (5) developed torque to rotor volume ratio of the motor can be calculated and can be expressed as:

$$k_{trv} = \frac{ac\pi k_w B_{air-gap}}{\sqrt{2}} \tag{6}$$

The slot area can be determined through the formula presented in Eq. (7). The relationship between the nominal current per phase and current density allows us to ascertain the copper conductor's area, which, in turn, can be employed to determine the radius of the conductor. By applying the assumed slot fill factor value, the total slot area of the motor can be calculated.

$$A_{slot} = \pi\left((R_{ro} - w_{bi})^2 - R_{si}^2\right) - N_s d_s w_t \tag{7}$$

$$A_{slot} = \frac{6N_{tph}A_{cond.}}{F_s} \tag{8}$$

Where, A_{slot} is the area of slot of the proposed motor, R_{so} is the stator outer radius, w_{bi} is the width of stator back iron, R_{si} is the stator inner radius can be calculated as the sum of length of air-gap and R_{ro}, d_s is the depth of slot, w_t is the width of the stator teeth and Acond. is the cross-sectional area of each conductor. Stator tooth width can be calculated using Eq. (9).

$$w_t = \frac{\pi\left((R_{ro} - w_{bi})^2 - R_{si}^2\right) - A_{slot}}{N_s d_s} \tag{9}$$

Table 1 displays the design specifics of the proposed 1 kW, 510 rpm motor. Fig. 1 shows the two-dimensional view of the proposed motor with the two-dimensional mesh and three-dimensional meshing. This 3-phase, 8-pole, 24-slot motor is taken into consideration as the reference motor for summarizing the cogging torque. For stator winding excitation, a 48 V supply is used. The rated torque developed by the motor is 18.8 N.m. The motor's length and outer diameter are 95.7 mm and 163 mm, respectively. And 5 mm thick permanent magnet poles with 31.5° magnet arc are mounted on the surface of the rotor. The rotor's inner and outer diameters are 70 mm and 107 mm, respectively. In the RF-BLDC motor, modelling and simulation are addressed for precise electromagnetic field analysis. Commercially accessible finite element software is used for modelling and simulation. None of the design techniques for cogging torque reduction are used on the reference motor.

Table 1. Design parameters and specifications [24].

Parameters	Value	Unit
Stator outer diameter	163	Mm
Length of motor	95.7	Mm
Stator inner diameter	108	Mm
Stator back iron depth	10.5	Mm
Stator tooth width	9	Mm
Air-gap length	0.5	Mm
Rotor outer diameter	107	Mm
Rotor inner diameter	70	Mm
Width of PM pole	5	Mm
No. of poles	8	-
No. of phases	3	-
No. of stator slots	24	-
Magnet fraction	0.7	-
Core material	M19-G29	-
Type of PM	NdFeB-35	-

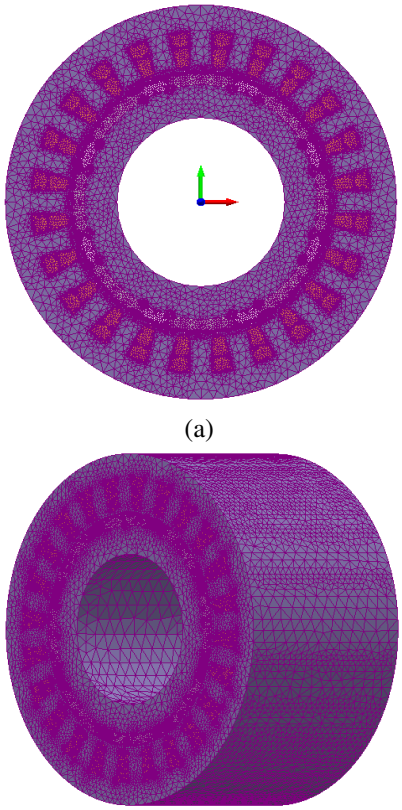

(a)

(b)

Fig. 1. Meshing view of the proposed 1000 W RF-BLDC motor.

Fig. 2-(a) shows the torque profile of the reference 1000 W motor with a torque ripple of 57% and an average torque of 18.8 N.m. The cogging torque profile of the proposed motor is presented in Fig. 2-(b). Because of the structural symmetry of the motor, the cogging torque variation is observed to be periodic with respect to the rotor position. The peak-to-peak cogging torque of the motor is 9.66 N.m. The flux density plot of the motor is shown in Fig. 3. The magnetic field strength remains uniform across the entire BLDC motor. The electromagnetic analysis output displays a spectrum of colours, with each shade indicating variations in magnetic field strength. The proximity between the assumed flux density and actual flux density in the respective section establishes the correctness of the initial design of the radial flux BLDC

motor. Table 2 juxtaposes the analytical outcomes with the finite element analysis (FEA) results of the 1000 W, 510 rpm RF-BLDC motor to authenticate the design. The performance estimation, executed using design parameters, that the projected performance parameters fall within acceptable thresholds. However, the slight disparity observed between the outcomes derived from the two methodologies may be attributed to the inherent variability in the design variables and equations employed in the analytical approach.

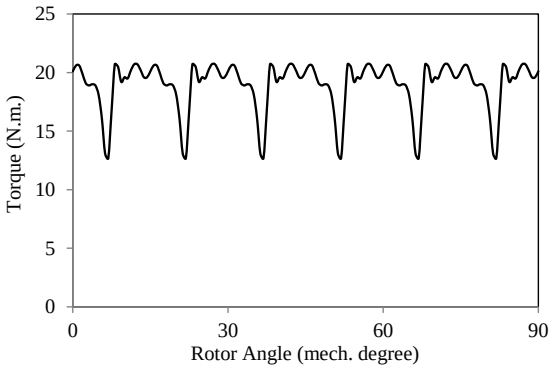

(a) Torque profile.

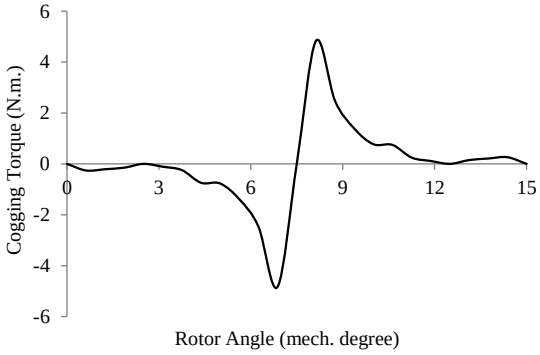

(b) Cogging torque profile.

Fig. 2. Torque profile and cogging torque profile of 1000 W reference RF-BLDC motor.

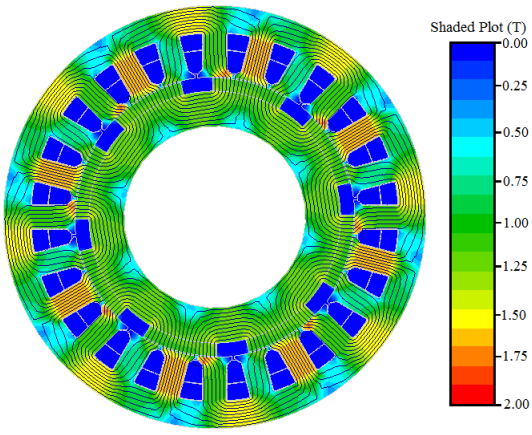

Fig. 3. Flux distribution plot of 1000 W reference RF-BLDC motor.

3. Cogging Torque in RF-BLDC Motor

In the RF-BLDC motor, the rotor pole has a tendency to align with the stator teeth while seeking the position of least magnetic reluctance; oscillatory torque occurs, known as cogging torque. This cogging torque manifests even when the stator winding of a BLDC motor is not energized. Hence, it is also known as detent torque or no current torque. Cogging torque depends on air-gap flux and air-gap reluctance variation as per Eq. (10). It is most visible at low speed, with the symptoms of jerks and noise. At high speed, the moment of inertia of the motor filters out jerks and vibration due to cogging torque. This can be expressed in detail using the following expression:

Table 2. Comparison of analytical and FEA based results for RF-BLDC motor.

Parameters	Unit	Analytical results	FEA results
Torque developed	N.m	18.76	18.8
Output power	T	1000	999.8
Flux density in stator back iron	T	1.5	1.53
Flux density in stator teeth	T	1.7	1.69
Flux density in rotor core	T	1.2	1.2

$$T_{cogging} = -\frac{1}{2}\phi_{gap}^2 \frac{dR_{gap}}{d\theta_r} \tag{10}$$

Where θ_r is the rotor angle, R_{gap} is air-gap reluctance and ϕ_{gap} is air-gap flux. The air-gap reluctance varies periodically as the rotor's angular position changes, generating a periodic cogging torque. Reducing reluctance variation or air-gap flux will lower both cogging torque and The only alternative for reducing cogging torque is to decrease air-gap reluctance variation because reducing air-gap flux derates the motor and is therefore not preferred. Cogging torque can be reduced by carefully choosing tooth edge inset width and magnet tip depth.

4. Reduction of Cogging Torque in RF-BLDC Motor

The interactions between the magnets and the stator tooth are additive because the magnets are in an identical relative position with regard to the tooth. A slight variation in design can lead to a change in air-gap flux, which directly affects the cogging torque of the motor. Hence, three approaches are proposed to reduce the cogging torque and improve motor performance.

4.1. Proposed teeth edge inset width variation technique

The teeth edge inset width variation technique is presented in Fig. 4, implemented on the stator teeth edge of the RF-BLDC motor. This proposed approach changes the tooth edge inset width instead of changing the width of the entire teeth shoe. Hence, this led to a reduction of the width of the wall on the slot opening side, as shown in Fig. 4. Due to the reduction in the width of the tooth edge inset width, less magnetic flux will enter from the sides of the tooth shoe. Thus, the magnitude of cogging torque as the tangential component of attraction force will be reduced [25].

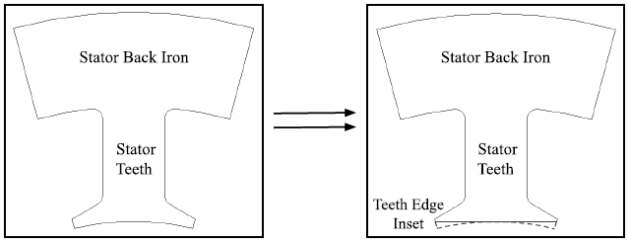

Fig. 4. Teeth edge inset width variation technique.

The width is changed from 0 to 0.35 mm. Using FEA, performance analysis was carried out for different values of TEIW.

The peak-to-peak cogging torque obtained for each variation is presented in Fig. 5. It is observed that at 0.35 mm TEIW, the peak-to-peak cogging torque is cut down to 5.0 N.m. from 9.66 N.m. Fig. 6-(a) compares the cogging torque profile of the reference model and the final model with the TEIW variation technique. With the application of TEIW, the variation torque ripple is reduced from 42.24% to 38.26%; Fig. 6-(b) shows the comparison of the torque profile of the reference and the improved model. The average torque of the motor is also slightly reduced with the application of this approach, but the reduction is found in the permissible band. The flux density plot of the motor improved with the application of the TEIW approach is shown in Fig. 7. The magnetic field strength remains uniform across the entire BLDC motor.

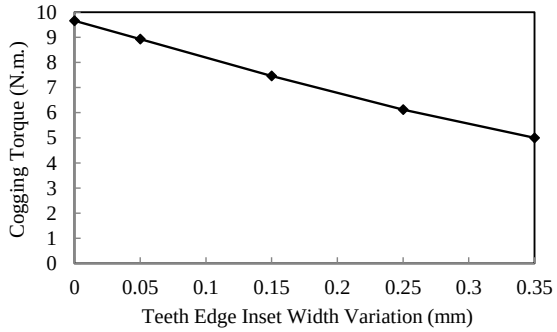

Fig. 5. Peak to peak cogging torque obtained at various TEIWs.

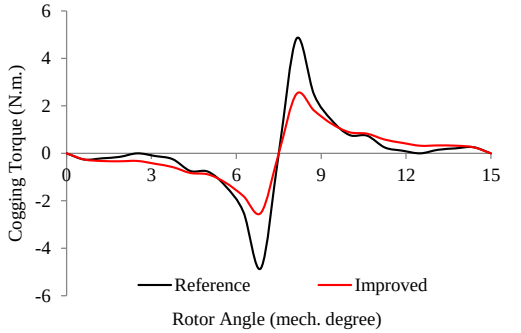

(a) Cogging torque profiles.

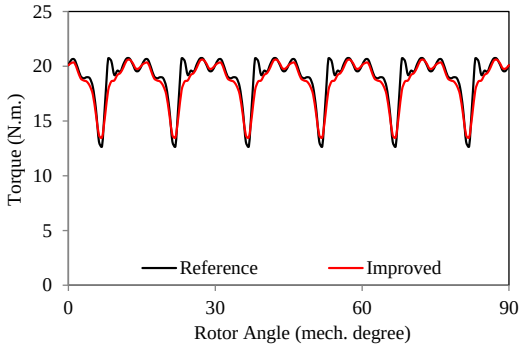

(b) Torque profiles.

Fig. 6. Cogging torque and torque profile comparison of the reference model and improved model with 0.35 mm TEIW.

4.2. Magnet tip depth variation technique

The magnet tip depth variation technique is presented in Fig. 8, which is implemented on the PM rotor poles of the RF-BLDC

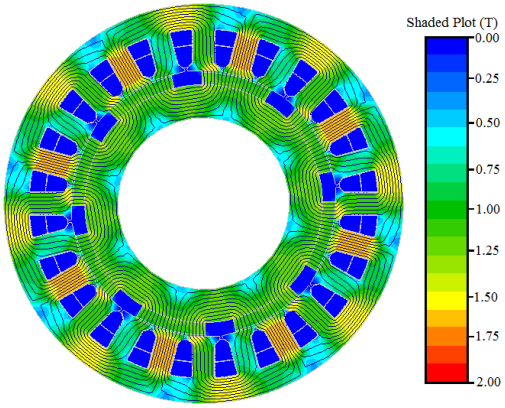

Fig. 7. Flux density plot of improved motor with 0.35 mm TEIW.

motor. In this approach, the tip of the permanent magnet pole is reduced instead of changing the width of the entire pole. This change in the depth of the magnet tip leads to a reduction of cogging torque as the tangential component of attraction force will be acting on the teeth compared to the initial permanent magnet pole [23]. The depth is changed from 0 to 0.8 mm without keeping all the other parameters unchanged. Using electromagnetic analysis software, a simulation was carried out of each variation from 0 to 0.8 mm with the step of 0.1 mm.

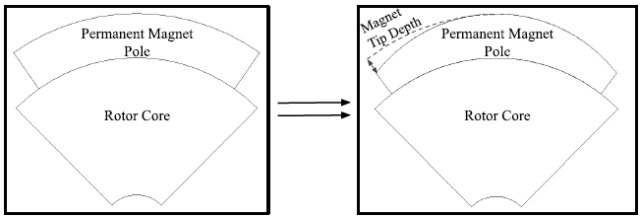

Fig. 8. Magnet tip depth variation technique.

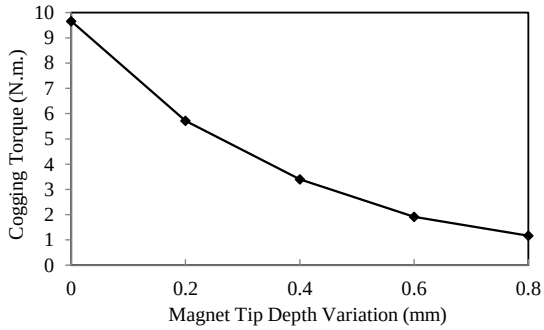

Fig. 9. Peak to peak cogging torque obtained at various MTDs.

The peak-to-peak cogging torque obtained for each variation is presented in Fig. 9. And Fig. 10-(a) compares the cogging torque profile of the reference model and the final model with the MTD variation technique. The minimum cogging torque is obtained at 0.8 mm. Fig. 10-(b) shows the torque profile compaction of the initial and the improved model with the MTD variation technique at a depth of 0.8 mm. It clearly shows a significant reduction in torque ripple. The average torque of the motor is also slightly reduced with the application of this approach, but the reduction is found in the permissible band. The flux density plot of the motor improved with the application of the MTD approach is shown in

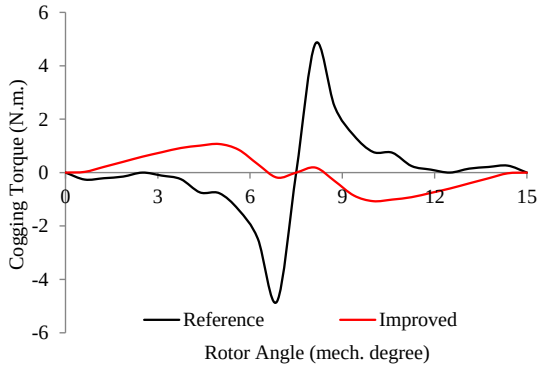

(a) Cogging torque profiles.

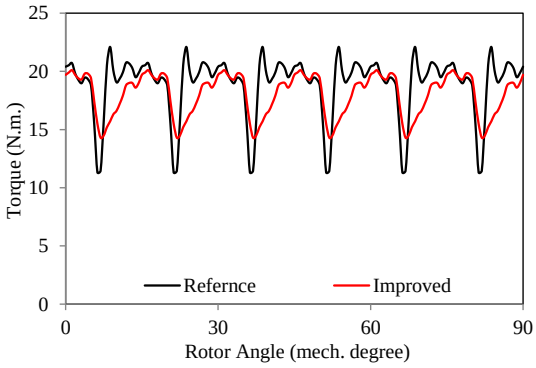

(b) Torque profiles.

Fig. 10. Cogging torque and torque profile comparison of the reference motor and improved motor with 0.8 mm MTD.

Fig. 11. The magnetic field strength remains uniform across the entire BLDC motor.

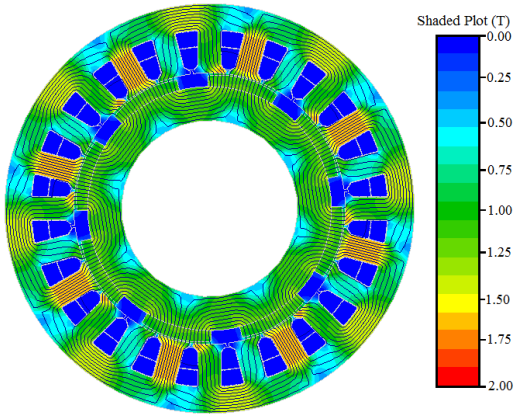

Fig. 11. Flux density plot of the improved motor with 0.8 mm MTD.

4.3. Proposed hybrid approach

This proposed hybrid approach involves variation on both the stator and the rotor side of the motor using the two techniques mentioned above: TEIW and MTD variation techniques. Using this approach reduces the complexity of excessive modification of any one part of the motor. A slight variation on one side in combination with the other side provided better results than any individual approach. This approach involves reducing cogging torque by employing various combinations of TEIW and MTD. Figs. 12-(a) and 12-(b) compare the cogging torque and torque profile of the reference model and the model improved with the hybrid approach, respectively. The torque ripple in the improved model is reduced to 29.70%, with a 90.68% reduction in peak-to-peak cogging torque.

Table 3 shows the selection of levels of two approaches (i.e.

Table 3. Variables with their respective levels for L_{16} orthogonal table.

Variables	Unit	Levels			
		Level 1	Level 2	Level 3	Level 4
A (Magnet tip depth)	mm	0.2	0.4	0.6	0.8
B (Tooth edge inset width)	mm	0.05	0.15	0.25	0.35

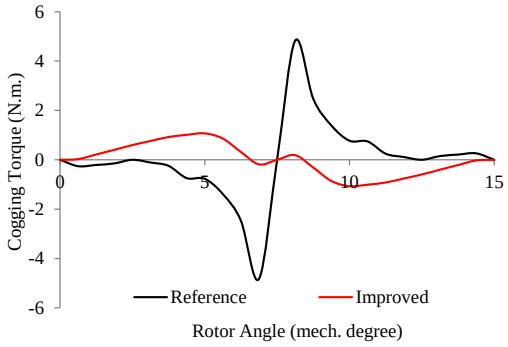

(a) Cogging torque profiles.

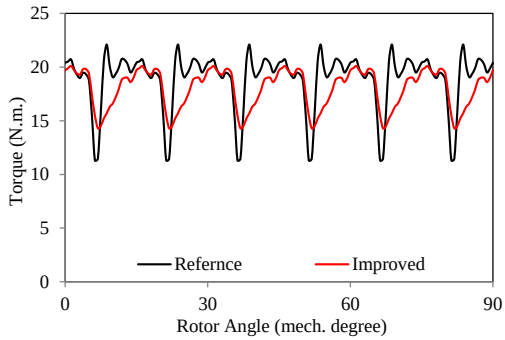

(b) Torque profiles.

Fig. 12. Cogging torque and torque profile comparison of the reference motor and improved motor with hybrid approach (0.8 mm MTD with 0.05 mm TEIW).

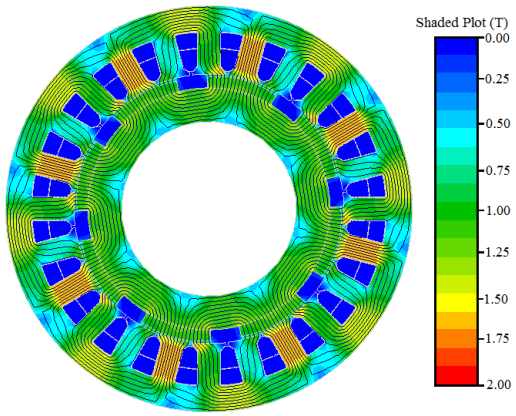

Fig. 13. Flux density plot of the improved model with hybrid approach (0.8 mm MTD with 0.05 mm TEIW).

Table 4. Orthogonal array [L_{16}] comparing performance parameters for each test run.

Test run	Variables A	Variables B	Cogging torque (N.m.)	Cogging torque reduction (%)	Average torque (N.m.)	Torque ripple (%)
1	1	1	5.25	45.34	18.67	35.88
2	1	2	4.32	55.27	18.56	35.01
3	1	3	3.46	64.18	18.46	34.12
4	1	4	2.74	71.63	18.34	33.81
5	2	1	3.10	67.90	18.46	33.03
6	2	2	2.44	74.74	18.24	32.71
7	2	3	1.86	80.72	18.24	32.34
8	2	4	1.35	86.00	18.13	31.98
9	3	1	1.69	82.50	18.24	31.23
10	3	2	1.22	87.37	18.13	30.88
11	3	3	1.41	85.36	18.02	31.06
12	3	4	1.78	81.61	17.91	31.25
13	4	1	0.90	90.68	18.02	29.96
14	4	2	1.45	84.96	17.91	30.69
15	4	3	1.93	80.04	17.80	30.88
16	4	4	2.42	74.92	17.71	31.64

Table 5. Performance comparison.

Parameters	Reference motor	Motor with TEIW approach	Motor with MTD approach	Motor with proposed hybrid approach
Cogging torque (N.m.)	9.66	5.00	1.16	0.90
Torque (N.m.)	18.8	18.55	18.07	18.02
Torque ripple (%)	42.24	38.26	29.87	29.4
Weight (kg)	11.40	11.375	11.360	11.360
PM weight (kg)	0.805	0.805	0.76	0.76

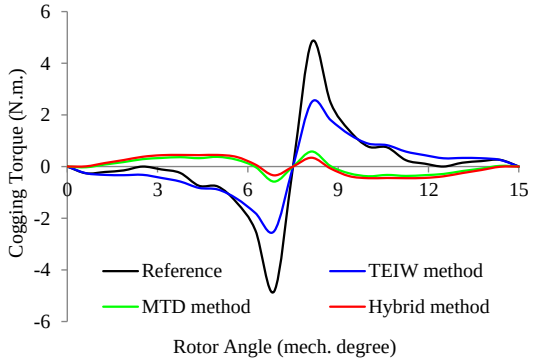

(a) Cogging torque profiles.

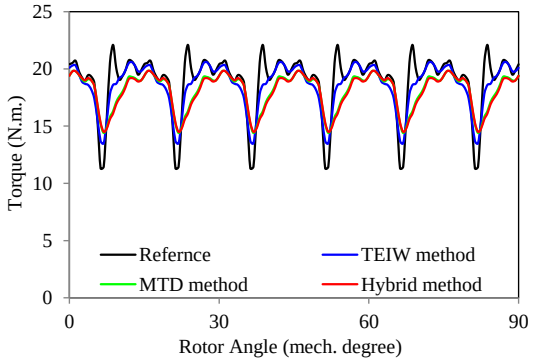

(b) Torque profiles.

Fig. 14. Cogging torque and torque profile comparison of the reference motor and improved motor with hybrid approach (0.8 mm MTD with 0.05 mm TEIW).

MTD variation and TEIW variation) for the formation on the L_{16} orthogonal table, as indicated in Table 4. It is evident that the peak-to-peak cogging torque decreases for all combinations using both methods. A more significant reduction in cogging torque is achieved with a high value of MTD and a lower value of TEIW, as shown in test run 13th in Table 4. This outcome is due to the smoother magnet edge provided by greater depth and a more uniform path for magnetic flux flow facilitated due to variation in TEIW shown in Fig. 13.

5. PERFORMANCE COMPARISON

This section discusses the comparison of the performance parameters obtained from the electromagnetic analysis of the different models designed and analysed in the above sections. Table 5 compares the performance of the TEIW variation approach, MTD variation approach and proposed hybrid approach with the reference motor. With improvement in only the stator side using the TEIW approach, the cogging torque is reduced by 48.24% with a reduction of 3.98% reduction in torque ripple. With the implementation of only the rotor side approach, which is the MTD variation approach, the cogging torque and torque ripple are reduced by 87.99% and 12.37%, respectively, compared to the reference motor. Both above-mentioned approaches reduce the cogging torque and torque ripple and also give the additional benefit of material requirement reduction, i.e., core material in the proposed TEIW variation approach and permanent magnet material in the proposed MTD variation. Now, with the application of the proposed hybrid approach, the peak-to-peak value of the cogging torque is cut down to 0.90 N.m. from 9.66 N.m. Torque ripple is reduced from 42.24% to 29.4% in the improved model. With the application of the proposed hybrid technique, the weight of the permanent magnet material is also reduced from 0.805 kg to 0.76 kg, along with the reduced requirement for core material. Figs. 14-(a) and 14-(b) compare the cogging torque and torque profile of all three techniques with reference design.

While the research effectively demonstrates the significant reduction in cogging torque using the three proposed techniques-teeth edge inset width (TEIW) variation, magnet tip depth (MTD) variation, and a hybrid of both-there are certain limitations to consider. The study primarily focuses on a specific motor configuration (1000 W, three-phase, 510 rpm RF-BLDC motor

with 24 slots and eight poles), which may limit the generalizability of the results to other motor types or configurations. Additionally, while the hybrid approach yielded the most substantial reduction in cogging torque, the complexity involved in its implementation might present challenges in mass production or in motors with different topologies. Future research could explore the application of the proposed techniques across a broader range of motor types and configurations. This could help us understand the versatility and scalability of the TEIW, MTD, and hybrid approaches. Advanced computational methods could also be employed to predict and further enhance the performance of these techniques. Lastly, integrating these approaches with modern manufacturing techniques could address the complexity of the hybrid method, making it more feasible for large-scale production.

6. Conclusion

This research focuses on the analysis and comparative evaluation of a 1000 W, three-phase, 510 rpm RF-BLDC motor, configured with 24 slots and eight poles. Three different approaches for reducing cogging torque are proposed and analyzed: teeth edge inset width variation (TEIW), magnet tip depth variation (MTD), and a hybrid of TEIW and MTD. These methods are scrutinized and compared to a reference configuration. The electromagnetic performance of these approaches was thoroughly examined. In the MTD approach, cogging torque was significantly reduced, along with a decrease in the demand for permanent magnet material compared to the reference design. Furthermore, all proposed approaches led to a reduction in peak-to-peak cogging torque relative to the reference design: 48.24% with the TEIW variation technique, 87.99% with the MTD variation technique, and 90.68% with the hybrid approach. This study unequivocally demonstrates the effectiveness of all proposed techniques in minimizing cogging torque. However, each method has its distinct advantages and constraints. Notably, the hybrid approach showed the most significant reduction in torque ripple, suggesting its potential suitability for a wide range of electric motor types with different topologies.

References

[1] Y.-P. Yang and D. S. Chuang, "Optimal design and control of a wheel motor for electric passenger cars," *IEEE Trans. Magn.*, vol. 43, no. 1, pp. 51–61, 2007.

[2] H. B. Duc, D. B. Minh, and V. D. Quoc, "Modeling of centrifugal stress and deformation of double v and delta layer of interior permanent magnet rotor design-application to electrical vehicles," *GMSARN Int. J.*, vol. 17, pp. 302–308, 2023.

[3] A. Cavagnino, M. Lazzari, F. Profumo, and A. Tenconi, "A comparison between the axial flux and the radial flux structures for pm synchronous motors," *IEEE Trans. Ind. Appl.*, vol. 38, no. 6, pp. 1517–1524, 2002.

[4] S. Arand, "Optimization of pm segments shift angles for minimizing the cogging torque of yasa-afpm machines using response surface methodology," *J. Oper. Autom. Power Eng.*, vol. 9, no. 3, pp. 203–212, 2021.

[5] T. Jhankal and A. N. Patel, "Design and cogging torque reduction of radial flux brushless dc motors with varied permanent magnet pole shapes for electric vehicle application," *Trans. Energy Syst. Eng. Appl.*, vol. 4, no. 2, pp. 1–13, 2023.

[6] N. Rostami, A. A. Kadhim, and M. B. Bannae-Sharifian, "Cogging force reduction in pmlsms using segmented magnets," *J. Oper. Autom. Power Eng.*, vol. 13, no. 3, pp. 206–211, 2025.

[7] R. Bansal, S. Marwaha, and C. Verma, "Cogging torque minimization of pmbldc motor for application in battery electric vehicle," *J. Electr. Eng. Technol.*, vol. 18, no. 3, pp. 1733–1743, 2023.

[8] L. Dosiek and P. Pillay, "Cogging torque reduction in permanent magnet machines," *IEEE Trans. Ind. Appl.*, vol. 43, no. 6, pp. 1565–1571, 2007.

[9] N. Bianchi and S. Bolognani, "Design techniques for reducing the cogging torque in surface-mounted pm motors," *IEEE Trans. Ind. Appl.*, vol. 38, no. 5, pp. 1259–1265, 2002.

[10] P. T. Luu, J.-Y. Lee, W. Hwang, and B.-C. Woo, "Cogging torque reduction technique by considering step-skew rotor in permanent magnet synchronous motor," in *2018 21st Int. Conf. Electr. Mach. Syst.*, pp. 219–223, IEEE, 2018.

[11] T. Anuja and M. A. N. Doss, "Reduction of cogging torque in surface mounted permanent magnet brushless dc motor by adapting rotor magnetic displacement," *Energies*, vol. 14, no. 10, p. 2861, 2021.

[12] Y.-H. Jung, M.-S. Lim, M.-H. Yoon, J.-S. Jeong, and J.-P. Hong, "Torque ripple reduction of ipmsm applying asymmetric rotor shape under certain load condition," *IEEE Trans. Energy Convers.*, vol. 33, no. 1, pp. 333–340, 2017.

[13] J. Liang, A. Parsapour, Z. Yang, C. Caicedo-Narvaez, M. Moallem, and B. Fahimi, "Optimization of air-gap profile in interior permanent-magnet synchronous motors for torque ripple mitigation," *IEEE Trans. Transp. Electrif.*, vol. 5, no. 1, pp. 118–125, 2019.

[14] C. Bharatiraja, M. Deepak, and D. Jagadeesh, "Finite element analysis of permanent magnet less motors for electric vehicle application," in *2023 Fifth Int. Conf. Electr. Comput. Commun. Technol.*, pp. 1–6, IEEE, 2023.

[15] Z. Ding, X. Wu, C. Chen, and X. Yuan, "Magnetic field analysis of surface-mounted permanent magnet motors based on an improved conformal mapping method," *IEEE Trans. Ind. Appl.*, vol. 59, no. 2, pp. 1689–1698, 2022.

[16] N. Rostami, A. A. Kadhim, and M. B. Bannae-Sharifian, "Cogging force reduction in pmlsms using segmented magnets," *J. Oper. Autom. Power Eng.*, vol. 13, no. 3, pp. 206–211, 2025.

[17] V. Naeini and N. Sadeghi, "Optimum design of the outer rotor brushless dc permanent magnet motor with minimum torque ripples," *J. Oper. Autom. Power Eng.*, 2024.

[18] P. R. Upadhyay and K. Rajagopal, "Fe analysis and computer-aided design of a sandwiched axial-flux permanent magnet brushless dc motor," *IEEE Trans. Magn.*, vol. 42, no. 10, pp. 3401–3403, 2006.

[19] B. Singh and D. Goyal, "Computer aided design of permanent magnet brushless dc motor for hybrid electric vehicle application," in *2006 Int. Conf. Power Electron. Drives Energy Syst.*, pp. 1–6, IEEE, 2006.

[20] S. H. Bibak, M. H. Mousavi, and M. Geravandi, "Design and electromagnetic analysis of brushless salient pole switching flux synchronous generator with dc auxiliary field winding for wind energy converter systems," in *2023 31st Int. Conf. Electr. Eng.*, pp. 160–166, IEEE, 2023.

[21] D. C. Hanselman, *Brushless permanent magnet motor design*. The Writers' Collective, 2003.

[22] J. R. Hendershot and T. J. E. Miller, *Design of brushless permanent-magnet motors*. Oxford university press, 1995.

[23] T. Jhankal and A. N. Patel, "Design and analysis of spoke type radial flux interior permanent magnet synchronous motor for high-speed application," in *2022 2nd Odisha Int. Conf. Electr. Power Eng. Commun. Comput. Technol.*, pp. 1–5, IEEE, 2022.

[24] T. Jhankal and A. N. Patel, "Design and cogging torque reduction of radial flux brushless dc motors with varied permanent magnet pole shapes for electric vehicle application," *Trans. Energy Syst. Eng. Appl.*, vol. 4, no. 2, pp. 1–13, 2023.

[25] C. Studer, A. Keyhani, T. Sebastian, and S. Murthy, "Study of cogging torque in permanent magnet machines," in *IAS'97. Conf. Record 1997 IEEE Ind. Appl. Conf. Thirty-Second IAS Annu. Meet.*, vol. 1, pp. 42–49, IEEE, 1997.